

# Supplemental Materials for **BiVO<sub>4</sub> thin film photoanodes grown by Chemical Vapor Deposition**

Esther Alarcon-Llado,<sup>a,b,c,\*</sup> Le Chen,<sup>a,c,\*</sup> Mark Hettick,<sup>a,c,d</sup> Neeka Mashouf,<sup>a</sup> Yongjing Lin,<sup>a,c,d</sup>  
Ali Javey<sup>a,c,d</sup> and Joel W. Ager,<sup>a,c</sup>

<sup>a</sup> Joint Center for Artificial Photosynthesis, 2929 7<sup>th</sup> Street, Berkeley, CA, USA. Fax: +01 510 486 4995; Tel: +01 510 486 6715.

<sup>b</sup> École Polytechnique Fédérale de Lausanne, LMSC-SMX, Station 12, Lausanne, Switzerland. Tel: +41 216936826.

<sup>c</sup> Materials Sciences Division, Lawrence Berkeley National Laboratory, 1 Cyclotron Road, Berkeley, CA, USA. +01 510 486 4995; Tel: +01 510 486 6715.

<sup>d</sup> Department of Electrical Engineering and Computer Sciences, University of California, Berkeley, Berkeley, California 94720, United States.

## Experiment setup

A detailed sketch of two-zone furnace used for the vapour transport CVD growth of BiVO<sub>4</sub> thin films is shown in **Fig. S1**. We used a 1.5 inch diameter size quartz tube. The tube was pumped down to 80 mTorr prior to deposition, and compressed air (99.99%) was used as the carrier gas and source of oxygen. The solid inorganic precursors V<sub>2</sub>O<sub>5</sub> powder and Bi pellets were placed in Zone I of the furnace and the substrate was placed in the centre of Zone II. Zone I was set at 900 °C in order to melt the solid precursors. V<sub>2</sub>O<sub>5</sub> powder was placed at the centre of Zone I and Bi pellets were placed closer to the insulation zone between Zone I and Zone II which has lower temperature, about 750 °C. Zone II was set at temperature between 420 °C to 500 °C for the precursor vapour carried by the air flow to condense and react into monoclinic BiVO<sub>4</sub> phase on the substrate. The temperature ramping up speed was set at 15 degrees/min for both Zone I and Zone II. There is also 20 minutes soak temperature at about 120 °C for Zone I to degas the V<sub>2</sub>O<sub>5</sub> powder.

The pump was kept functioning for the whole growth process. With 1.5 inch diameter tube and full pump speed, we obtained 5.5 Torr with 200 sccm flow rate, 7.7 Torr with 200 sccm flow rate and 10 Torr with 300 sccm. After deposition, both the pump and the furnace were turned off right away in order to prevent excess deposition from any residual precursors. The system was vented to atmospheric pressure after cooling down to room temperature.

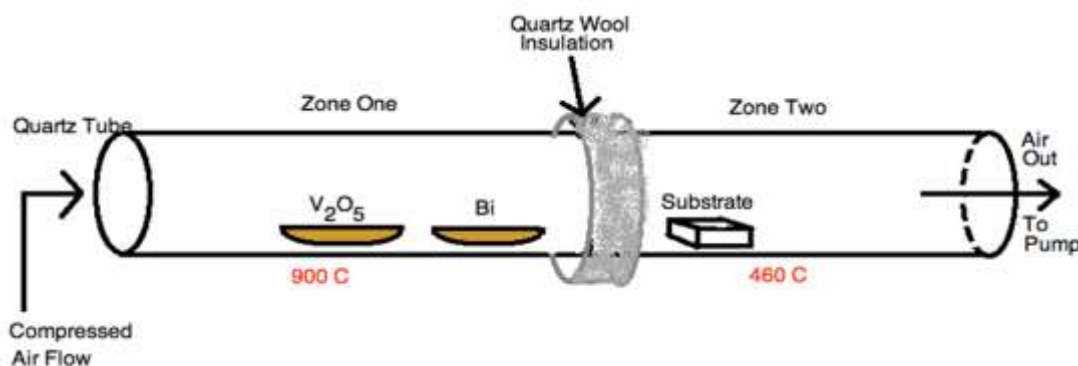


**Fig. S1.** Sketch of the CVD system. At an air flow rate of 200 sccm, the pressure in the deposition zone was 7.8 Torr.

## Growth limit

Films were grown for 2 hours using a Zone I temperature of 900 °C. The Zone II temperature was varied between 420 and 500 °C. We found that BiVO<sub>4</sub> growth using this method is self-limiting due to changes in the precursors as the growth progresses. A portion of the V<sub>2</sub>O<sub>5</sub> precursor is reduced during the process, becoming a mixture of oxygen poor compounds with a much higher melting point that eventually cannot contribute to BiVO<sub>4</sub> growth under the set conditions. Therefore, not all of the V<sub>2</sub>O<sub>5</sub>

loaded into the reactor will become  $\text{BiVO}_4$ . On the other hand, the Bi metal seems to be partially oxidized throughout the growth process; a residual crystallized yellow compound in the Bi boat suggests either  $\text{Bi}_2\text{O}_3$  or Bi-V-O formation.

### *Substrate pretreatment*

We explored the effect of substrate pre-treatment on the nucleation of the  $\text{BiVO}_4$  films. The substrates used were fluorine doped tin oxide on glass. **Figure S2** shows SEM micrographs depicting the surface coverage for untreated FTO, FTO cleaned with isopropyl alcohol (IPA) just prior to growth, and FTO clean with oxygen plasma generator and rinsed with IPA. The surface coverage is clearly improved by surface pretreatment, with the  $\text{O}_2$  plasma/IPA treatment yielding a more continuous and dense film.

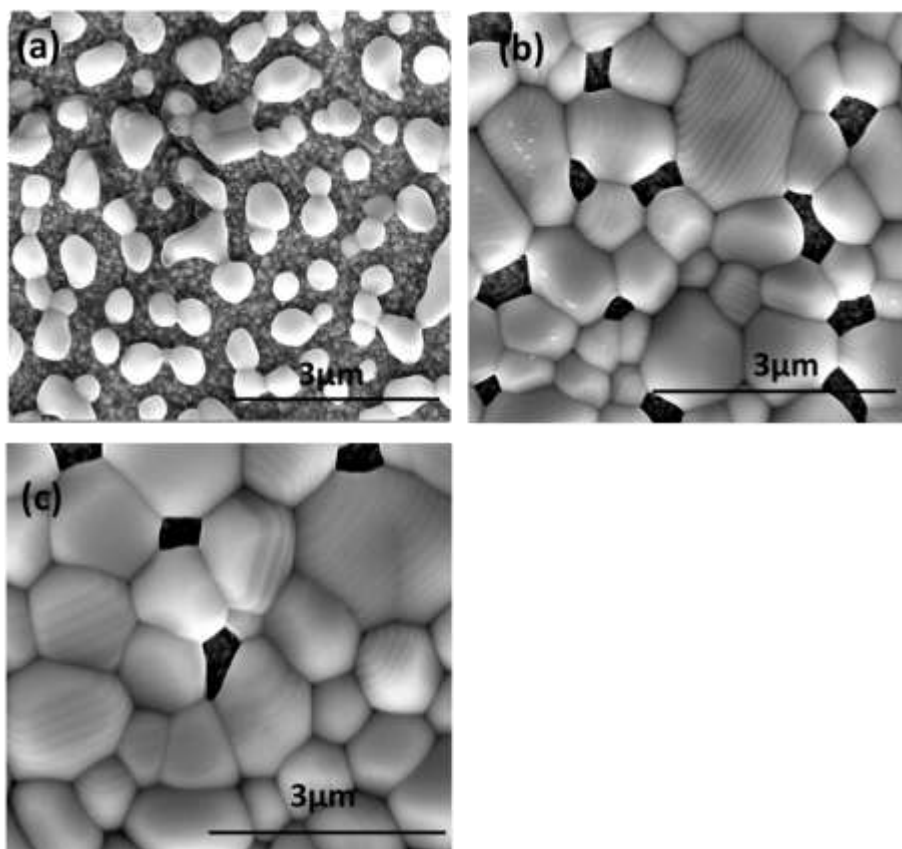


**Fig. S2.** Comparison of surface coverage for 3 treatments of the FTO/glass substrates prior to CVD growth of  $\text{BiVO}_4$ . A continuous and dense film is produced after an  $\text{O}_2$  plasma treatment of the FTO/glass substrate followed by a rinse in IPA prior to growth.

### *Crystalline structure*

CVD grown films were probed by Raman spectroscopy for revealing the crystalline structure as well as possible secondary phase formation. Here is a summary of a few Raman spectra of naturally formed bismuth vanadate minerals: pucherite (orthorhombic), dreyerite (tetragonal-scheelite) and clinobisvanite (monoclinic-scheelite). The Raman spectra of the minerals were obtained from the

RRUFF<sup>1</sup> database and are shown in **Fig. S3a**. One can easily observe the spectral differences between the orthorhombic and the other polymorphs. The spectra of the tetragonal and monoclinic phases, dreyerite and clinobisvanite respectively, are more alike. However, there are still some characteristic features that allow to distinguish between the two phases. The CVD-grown films can be concluded to be in the monoclinic phase due to the absence of a peak at 245 cm<sup>-1</sup>, as well as the presence of a single band at 829cm<sup>-1</sup>.

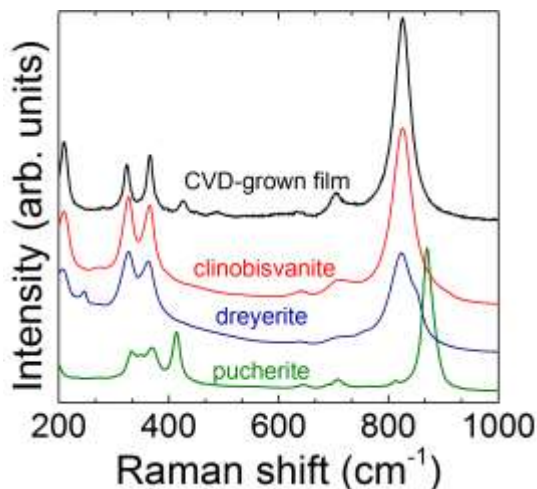


**Figure S3a.** Raman spectra of a representative CVD-grown film along with spectra from 3 BiVO<sub>4</sub> polymorphs obtained from the RRUFF database: pucherite (orthorhombic), dreyerite (tetragonal-scheelite) and clinobisvanite (monoclinic-scheelite),

As for the secondary phases that may form in our CVD films, vanadium and bismuth oxides could be expected. While the Raman spectrum of VO<sub>2</sub> presents very sharp peaks, Bi<sub>2</sub>O<sub>3</sub> polymorphs exhibit broader and simpler Raman spectra. A summary of those characteristic peaks can be found in the table below.

	VO <sub>2</sub>	V <sub>2</sub> O <sub>5</sub>		Bi <sub>2</sub> O <sub>3</sub>		
Crystalline structure	Tetragonal	Orthorhombic (α)	Tetragonal (β)	Monoclinic (α)	Tetragonal (β)	Cubic (γ)
Characteristic Raman peaks within 200-1000 cm <sup>-1</sup>	226, 260, 311, 337, 389, 438, 493, 595, 615, 627	289, 308, 406, 481, 532, 697, 993	211, 230, 244, 271, 285, 301, 340, 357, 434, 476, 574, 686, 736, 942	210, 280, 314, 413, 447, 529	311, 462	320, 550
reference	P. Schielbe, Phys. B 316, 600 (2002)	C. V. Ramana et al., Surf. Interface Anal. 37, 406 (2005)	R. Boaddour et al., Inorg. Chem. 51, 3194 (2012)	V. N. Denisov et al., J. Phys. Cond. Matt. 9, 4967 (1997)	F. D. Hardcastle et al., J. Solid State Chem. 97, 319 (1992)	F. D. Hardcastle et al., J. Solid State Chem. 97, 319 (1992)

From the Raman spectrum, we have only been able to observe the presence of α-V<sub>2</sub>O<sub>5</sub> forming in films grown under large air flow or low temperature conditions along with the BiVO<sub>4</sub>, as shown in **Fig. S3b**.

<sup>1</sup> The RRUFF project consists on a database on Raman, X-Ray and chemistry data of minerals. [www.ruff.info](http://www.ruff.info)

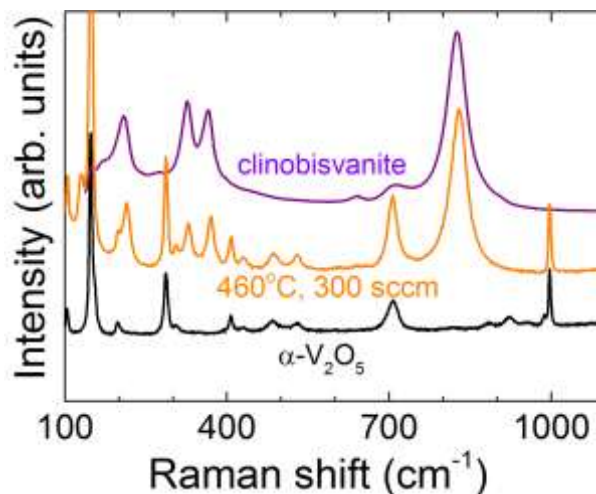


**Figure S3b.** Raman spectra of a CVD grown film under 460°C and 300 sccm of air flow. The spectrum is compared to that of monoclinic BiVO<sub>4</sub> (clinobisvanite) and orthorhombic V<sub>2</sub>O<sub>5</sub>.

### *The effect of synthesis conditions and substrate underlayers*

The purpose of this study was to synthesize stoichiometric BiVO<sub>4</sub> monoclinic sheelite films. In initial trials, we adjusted the locations of precursors and substrates as well as the amount of precursor used to achieve roughly stoichiometric films. For our reactor, when Zone II temperature was set at 460 °C and air pressure at 7.7 Torr (air flow 200 sccm), we could reliably obtain stoichiometric BiVO<sub>4</sub> using 0.65 g of Bi metal placed 1.8 cm from the reactor center (the center of the two zones) and 0.73 g V<sub>2</sub>O<sub>5</sub> 2.2 cm from reactor center (**Fig. S1**).

Then, we kept the precursor amount and location constant, and studied the effect of air flow as well as Zone II temperature on the stoichiometry of the films. We used three different settings for air flow: 100 sccm, 200 sccm and 300 sccm respectively and Zone II temperature was set at 460 °C). Under air pressure of 100 sccm, the product was mainly Bi<sub>2</sub>O<sub>3</sub> with poor coverage and under air pressure of 300 sccm, the product showed very vanadium rich condition (more than 60% of V measured by EDS) with phase separation of V<sub>2</sub>O<sub>5</sub> and BiVO<sub>4</sub>. Stoichiometric BiVO<sub>4</sub> thin film was obtained under 200 sccm air pressure. Regarding to Zone II temperature, we used 420 °C, 460 °C and 500 °C. Unlike air flow which has dramatic impact on the stoichiometry of the final products, Zone II temperature provides fine-tuning of the stoichiometry of the films. We were able to obtain slightly V-rich BiVO<sub>4</sub> films at Zone II temperature of 420°C, slightly Bi rich BiVO<sub>4</sub> films at Zone II temperature of 500 °C and stoichiometric BiVO<sub>4</sub> films at Zone II temperature of 460°C. The SEM images and related discussion of these three films are described in the main manuscript.

In addition, we explored the different effect of underlayers. We deposited samples on: 1) plain fluorine doped tin oxide (FTO, 25 Ω/□) 2) two layers of 1% Mo-doped BiVO<sub>4</sub> drop casted uniformly on FTO and dried at 150°C for a few minutes 3) 40 nm sputtered SnO<sub>2</sub> on FTO and 4) a combination of the latter. The detailed characterization results are showed and discussed in the main manuscript as well. **Figure S4** shows XPS analysis spectrum of Mo 3d of the sample with 1% Mo-doped BiVO<sub>4</sub> underlayers and there is no Mo detected at the surface of the sample showing that the CVD-grown film coverage is complete.

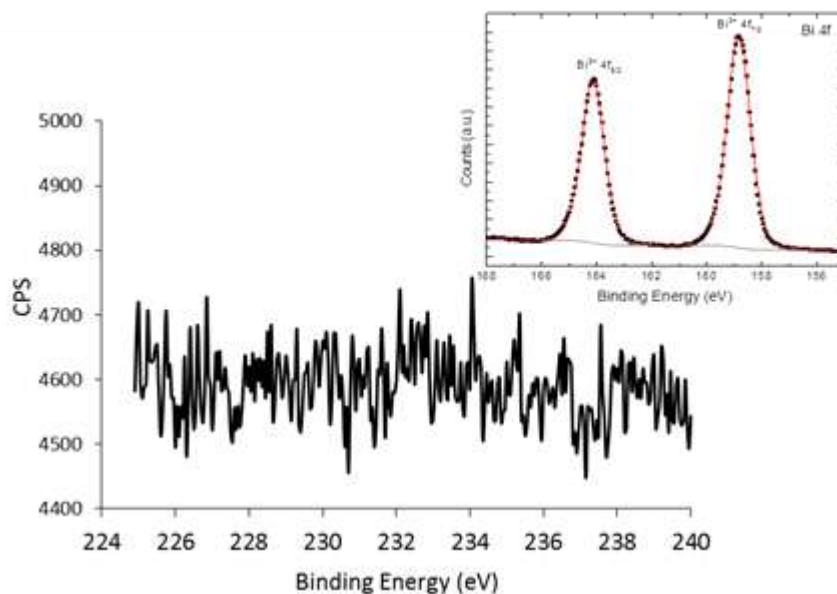


**Fig S4.** Narrow scan x-ray photoelectron spectra in the Mo 3d region of the  $\text{BiVO}_4$  sample with 1% Mo-doped  $\text{BiVO}_4$  underlayers. In comparison, an inset of Bi 4f spectra of the sample is shown. An Mo 3d signal is not observed, indicating that the coverage of  $\text{BiVO}_4$  by CVD growth is complete.

### *$\text{BiVO}_4$ deposited on ITO substrates*

We performed initial studies using ITO/glass substrates. **Figure S5(a)** shows the JV curves of a CVD film on ITO compared to a film grown on FTO with similar conditions. The PEC experiments are done in a solution containing  $\text{Na}_2\text{SO}_3$ . The PEC performance is very similar in both films.

As mentioned in the main text, the difference between front and back illumination is small also in thin films on ITO substrates, as represented in **Fig. S5(b)**. The JV curves correspond to a 100 nm-thick  $\text{BiVO}_4$  film grown on ITO/glass.

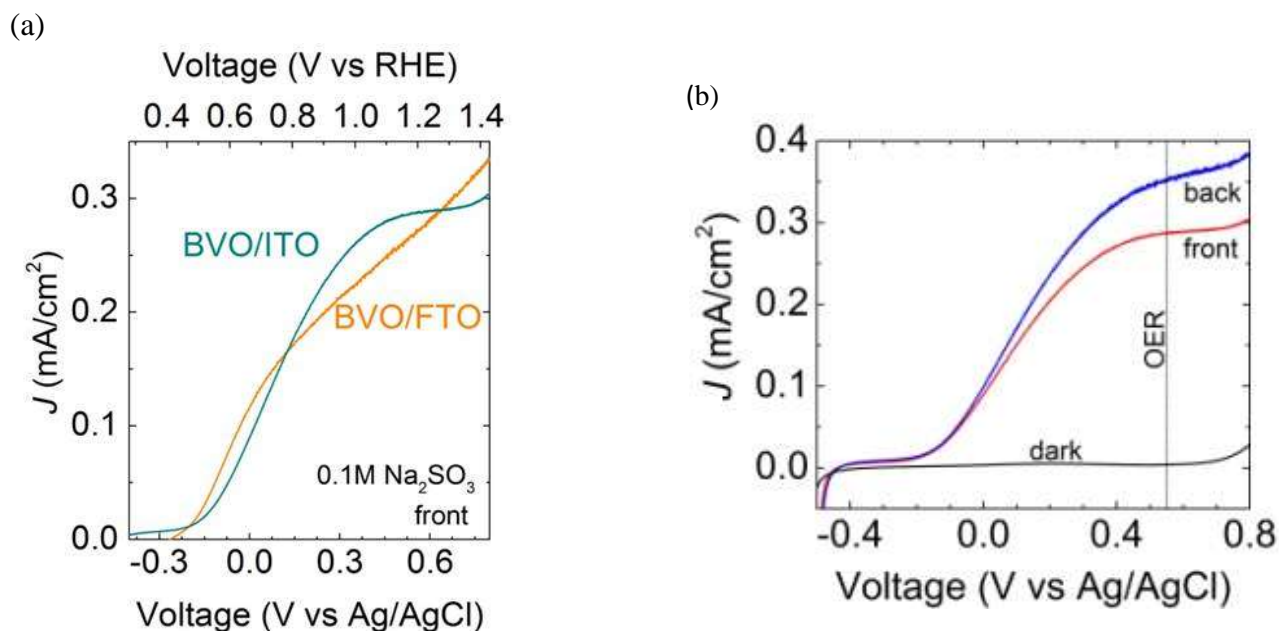


**Fig S5.** (a) JV curves of BiVO<sub>4</sub> thin film CVD deposited on ITO and FTO conducting substrates tested in pH 7 Na<sub>2</sub>SO<sub>3</sub> buffer solution and front illumination. (b) Comparison of JV curves of 100 nm BiVO<sub>4</sub> thin film CVD deposited on ITO conducting substrates tested in pH 7 Na<sub>2</sub>SO<sub>3</sub> buffer solution from back and front illumination.

### SEM image of BiVO<sub>4</sub> on Mo-doped BiVO<sub>4</sub>/SnO<sub>2</sub>/FTO

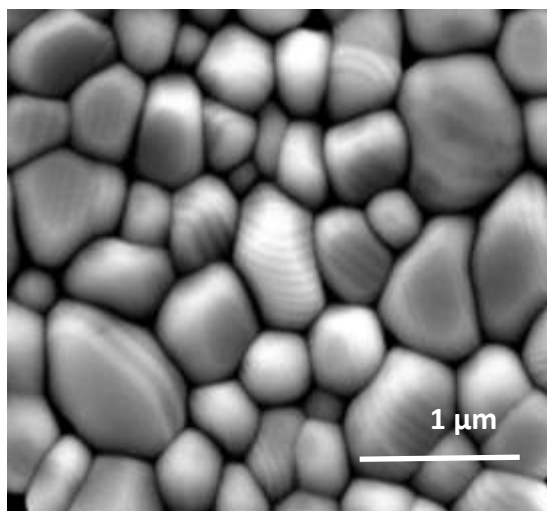


**Fig. S6.** SEM image of CVD deposited BiVO<sub>4</sub> on Mo-doped BiVO<sub>4</sub>/SnO<sub>2</sub>/FTO substrate.

In **Fig. S6** we show the SEM image of a CVD deposited film of BiVO<sub>4</sub> on Mo-doped BiVO<sub>4</sub>/SnO<sub>2</sub>/FTO substrate and the crystal size and film morphology is very similar to BiVO<sub>4</sub> on Mo-doped BiVO<sub>4</sub>/FTO shown in the manuscript.

### AFM image of $\text{BiVO}_4$ on Mo-doped $\text{BiVO}_4/\text{SnO}_2/\text{FTO}$

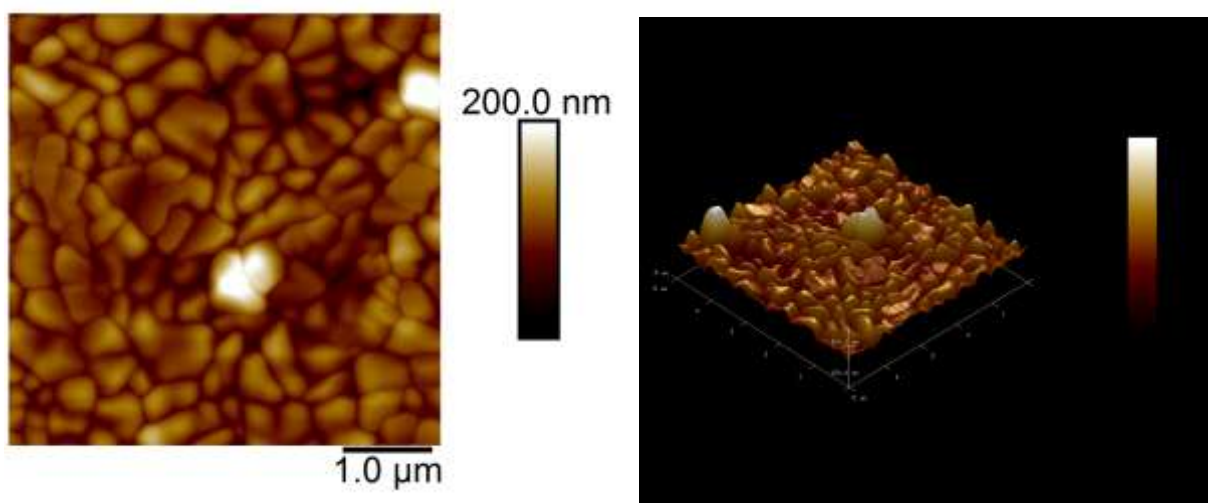


**Fig. S7.** Atomic force microscope (AFM) image (top view and 3D topography) of CVD deposited  $\text{BiVO}_4$ .

In **Fig. S7** the surface morphology of a CVD deposited film (compare **Fig. S6**) is characterized by atomic force microscopy (AFM). Surface roughness is extracted as 16.7 nm RMS, and voiding behavior is not evident in this image.

### Optical properties: reflectance and transmission

The CVD-grown thin films obtained were highly reflective ( $\sim 35\%$ ) as shown in **Fig. S8a**. We also show in **Fig S8b** the transmission spectra of a reference FTO/glass substrate, drop-casted Mo-doped  $\text{BiVO}_4$  underlayer on FTO/glass and a CVD-grown film on the previous structure. The thin (less than 20 nm) Mo- $\text{BiVO}_4$  underlayer is shown to absorb very little light as compared to the bulk  $\text{BiVO}_4$  film. Thus, the contribution of this underlayer for overall PEC performance is negligible.

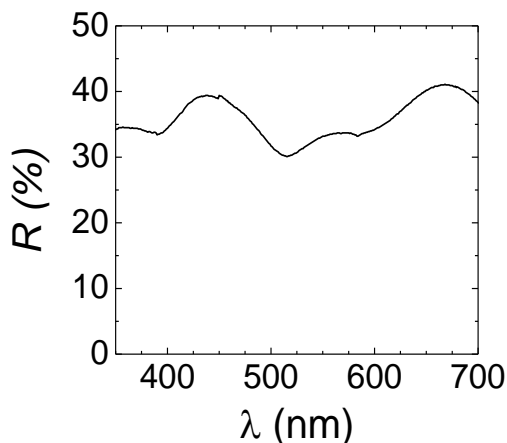


**Fig S8a.** Reflectance spectrum of a typical CVD grown  $\text{BiVO}_4$  film.

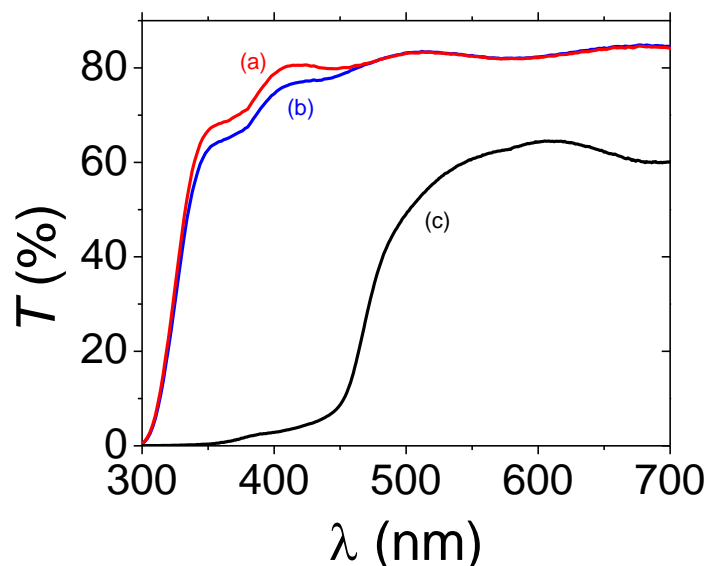


**Fig S8b.** Transmittance spectrum of a CVD grown  $\text{BiVO}_4$  film on FTO (c) in comparison with (a) FTO substrate and (b) 2 layers of Mo-doped  $\text{BiVO}_4$  (<20 nm) on FTO.

### Charge separation efficiency calculation

The photocurrent in a cell with the presence of a sacrificial reagent ( $\eta_{\text{cat}} = 1$ ) can be described as

$$J_{\text{photocurrent}} = J_{\text{absorbed}} \times \eta_{\text{charge separation}}$$

where  $J_{\text{absorbed}}$  is obtained by convolving the solar spectrum with the absorbance of the film. In order to be consistent with our experiments, we have used the spectrum from the solar simulator to perform our calculations. The films in this study are of similar thickness and have similar reflectance properties (see **Fig S8a**) so that  $J_{\text{absorbed}}$  is almost the same for all cases, ca.  $2.7 \text{ mA/cm}^2$ . We note that this value represents the maximum photocurrent possible for our films and is small compared to some experimentally reported values in the literature. This is mostly due to the large reflectance of our films.

Similarly, the incident photon to current efficiency (IPCE) is proportional to the light harvesting efficiency ( $\eta_{\text{light}}(\lambda)$ ), charge separation efficiency ( $\eta_{\text{CS}}(\lambda)$ ) and collection efficiency ( $\eta_{\text{cat}}$ ). The relationship is

$$\text{IPCE}(\lambda) = \eta_{\text{light}}(\lambda) \eta_{\text{CS}}(\lambda) \eta_{\text{cat}}$$

where  $\eta_{\text{light}}(\lambda)$  is related to the optical properties of the photoanode. Both reflectivity and absorption are taken into account here. In fact, from the UV-VIS experiments, one can directly obtain  $\eta_{\text{light}}(\lambda)$  from  $(1-R)(1-e^{-\alpha d})$ , being  $R$  the reflectance,  $\alpha$  the absorption coefficient, and  $d$  the film thickness, as shown in **Fig. S9**.

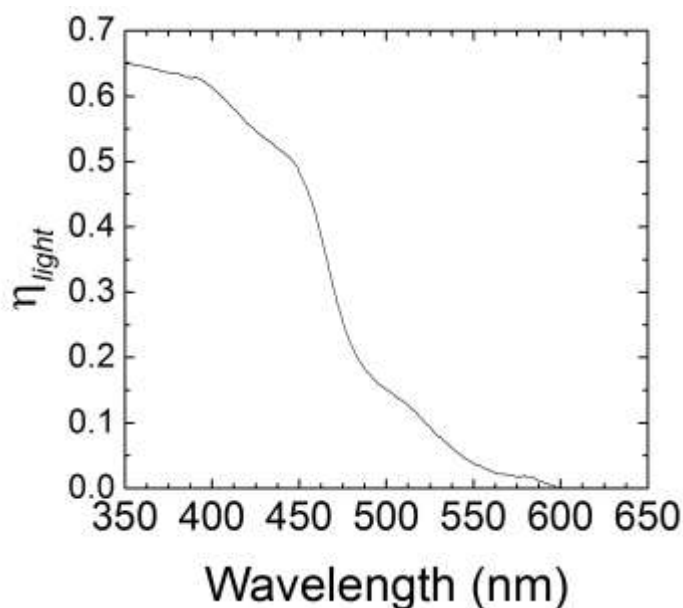


**Fig S9.** Light absorption efficiency from a representative sample

On the other hand, the collection efficiency at the liquid-semiconductor interface is a matter of its catalytic properties. Because in our experiments a sacrificial reagent was used, we expect  $\eta_{cat}$  to be close to 1. Consequently, by using the optical properties of the photoanodic films, the IPCE can be directly related to the charge separation efficiency, which in turn is linked to the electrical properties of the photoanode and to the collection efficiency at the back contact interface. The charge extraction efficiency  $\eta_{sep}$  as a function of wavelength is shown in **Fig. S10**. As with the overall photocurrent, modification of the back contact improves the charge separation efficiency.

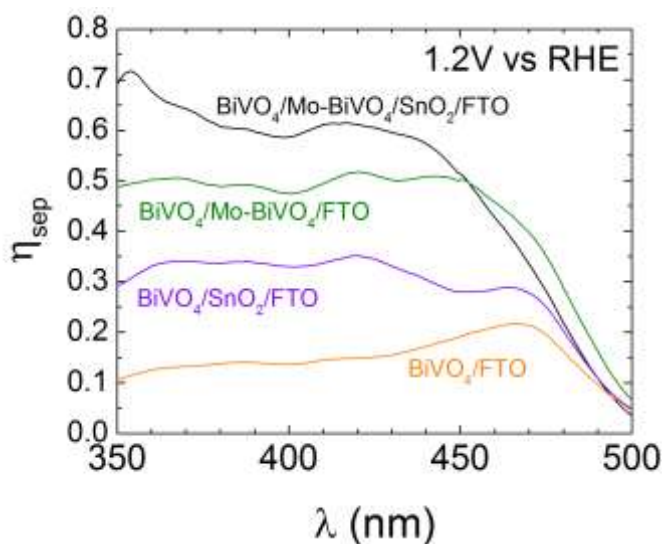


**Fig S10.** Charge separation efficiency as a function of wavelength as obtained from the IPCE and optical measurements.